Björn Karl Licht*, Fabian Homeyer, Katharina Bösebeck, Michael Binnewies, and Paul Heitjans

Synthesis and Electrochemical Behavior of Nanostructured Copper Particles on Graphite for Application in Lithium Ion Batteries

DOI 10.1515/zpch-2015-0003
Received January 16, 2015; accepted August 1, 2015

Abstract: Graphitic materials are currently the state-of-the-art anode materials for lithium ion secondary batteries. By chemical modification, the electrochemical performance of the pristine materials can be improved. In this paper we report on the preparation of nanostructured copper particles on graphite by thermal decomposition of copper formate. With this technique a novel, simple and low cost method for a homogeneous deposition of nanostructured copper particles on graphite was established. Different amounts of copper were realized and their influence on the electrochemical behavior of the active material was investigated. The copper particles had a size distribution between 50 nm and 300 nm. Electrochemical measurements displayed an improved performance of the synthesized composite material compared to the pristine material. Cyclic voltammetry showed a suppressed cointercalation of solvated lithium and an increased formation of the solid electrolyte interphase (SEI). Battery cycling demonstrated an increased discharge capacity and cycling stability.

***Corresponding author: Björn Karl Licht,** Leibniz Universität Hannover, Institut für Anorganische Chemie, Callinstr. 9, 30167 Hannover, Germany, e-mail: bjoern.licht@aca.uni-hannover.de
Fabian Homeyer: Leibniz Universität Hannover, Institut für Anorganische Chemie, Callinstr. 9, 30167 Hannover, Germany
Katharina Bösebeck: Leibniz Universität Hannover, Institut für Physikalische Chemie und Elektrochemie, Callinstr. 3–3a, 30167 Hannover, Germany
Michael Binnewies: Leibniz Universität Hannover, Institut für Anorganische Chemie, Callinstr. 9, 30167 Hannover, Germany; and Leibniz Universität Hannover, ZFM – Zentrum für Festkörperchemie und Neue Materialien, Callinstr. 3–3a, 30167 Hannover, Germany
Paul Heitjans: Leibniz Universität Hannover, Institut für Physikalische Chemie und Elektrochemie, Callinstr. 3–3a, 30167 Hannover, Germany; and Leibniz Universität Hannover, ZFM – Zentrum für Festkörperchemie und Neue Materialien, Callinstr. 3–3a, 30167 Hannover, Germany

Keywords: Li-ion Battery, Graphite Anode, Nanostructured Copper, Surface Modification, Cycle Stability, Thermal Decomposition.

1 Introduction

Energy storage is a key interest of modern society. On the one hand efficient storage devices are required to accumulate the energy from discontinuously available, green energy sources such as wind, sun or water. On the other hand there is a demand for batteries with a high capacity to power electric vehicles and mobile devices such as mobile phones and laptops [1]. The state-of-the-art secondary batteries for the majority of these applications are lithium ion batteries (LIBs) [2, 3]. In particular, electric vehicles require a considerably higher energy density than commercially available LIBs nowadays can provide [4]. Therefore, further investigations and improvements are needed.

Currently, lithium intercalating graphitic materials are utilized as anode material in most commercial lithium ion batteries [5, 6]. While graphite possesses only about 8% of the gravimetric energy density of metallic lithium, these materials are preferred due to safety reasons, low cost, good availability and their environmental friendliness. Nevertheless, graphite anodes show some disadvantages. During charge/discharge cycling or storage of LIBs, aging effects may occur [7]. Mechanical degradation like graphite exfoliation or surface structural disordering leads to loss of mobile lithium or self-discharge [8–11]. One of the main reasons for exfoliation is the cointercalation of solvated lithium ions. This causes a 200% higher volume increase compared to the intercalation of unsolvated lithium ions, which leads to mechanical stress in the electrode material [12]. An often discussed phenomenon related to the topic of aging effects is the formation of the solid electrolyte interphase (SEI), a protective layer of organic and inorganic lithium salts. Even though it is not completely understood yet, it is assumed that the SEI protects the anode from massive cointercalation of solvated lithium ions [13, 14]. A widely-used strategy to prevent aging effects and therefore improve the charge/discharge cycle life and stability of graphite anodes is the coating of graphite particles, e.g. with a secondary carbon shell, metal oxides or metals [15–18].

One method of metal coating on graphite was presented by Guo et al. [19]. It resulted in superior electrochemical properties of the material, such as an increased electric conductivity and therefore improved high rate capability [20, 21]. It was noted that possible reasons for the observed improvements are the suppression of solvent cointercalation and an improved lithium ion charge transfer at the graphite/electrolyte interface [19]. This leads to an increased cycle life perfor-

mance. Low sensitivity to adsorption of water/moisture compared to the pristine material was also described in literature [22]. Moisture can lead to the formation of hydrogen fluoride (HF) due to the reaction with the commonly used conducting salt lithium hexafluorophosphate ($LiPF_6$) [23]. Additionally, the usual conditions in a lithium ion battery will cause the decomposition of water into the elements.

Although the presented measurements show promising results, there is still room for further improvement. The major drawbacks of the reported coating methods are their high costs, the complexity of the processes, the usage of harmful chemicals (e.g. formaldehyde) and the influence of obtained byproducts [19, 20]. Due to the disadvantages mentioned above copper coatings are, to our knowledge, not yet applied in commercial applications. Therefore, our aim is to develop an environmentally friendly, simple and low cost procedure to deposit pure metal coatings on inorganic substances. It is well known that some metal formates sublimate and decompose at relatively low temperatures [24]. The exact chemical composition of the decomposition products is still not confirmed and varies for each metal formate. Based on this knowledge, a novel synthesis route for the preparation of homogeneous copper depositions on graphite is shown. The synthesis proceeds via a gas phase reaction by the thermal decomposition of copper formates. In addition, the long-term cyclability of copper coated graphite was not yet investigated, charge/discharge cycling was only performed up to 25 cycles [19, 20]. For any of the above mentioned applications this is insufficient. In this work a long-term 200 cycle charge/discharge measurement is presented.

We finally mention the well known fact that small scaled copper particles can be used as catalysts in various oxidation and reduction reactions, such as the reduction of NO_x [25] or in the synthesis of methanol [26, 27]. Thus, the synthesis route published here may also be employed to prepare pure metal depositions with possible catalytic applications.

2 Synthesis of nanostructured copper particles on graphite

Ordinary synthetic flake graphite (SGL CARBON, D10: 4.2 µm, D50: 21.9 µm, D90: 50.0 µm, BET surface area: $1.94\ m^2 \cdot g^{-1}$) and copper formate ($Cu(HCOO)_2 \cdot 4H_2O$, Alfa Aesar, 98%) were mixed and homogenized in a Retsch mixer mill MM 200 at a frequency of 20 Hz for 1 h.

Figure 1 shows the schematic experimental setup. The reaction tube, made of fused quartz, is inserted into a tube furnace. Argon is brought in at one end of the reaction tube. At the other end a drying system is installed to prevent contamina-

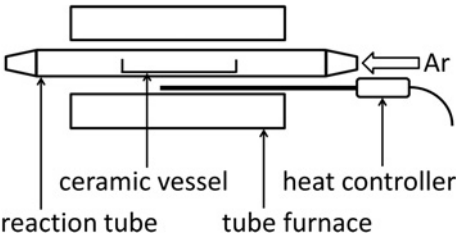

Figure 1: Schematic experimental setup of the reaction tube and the hot wall furnace used for the synthesis of the nanostructured copper particles on graphite.

tion with water. Prior to the experiment, the reaction chamber was flushed with argon gas. The powder blend was transferred into a ceramic vessel which was inserted into the reaction chamber. The furnace was heated to 100 °C for 30 min and subsequently to 300 °C for 1 h. Gaseous byproducts were removed by a constant argon flow. The content of copper on the graphitic surface is proportional to the amount of $Cu(HCOO)_2 \cdot 4H_2O$ used in the synthesis. Amounts of copper on graphite between 2.7 wt. % and 24.3 wt. % were realized.

3 Analytic techniques

The prepared composite materials as well as the pristine material were characterized by several analytic methods. Thermogravimetric measurements (TG) and differential scanning calorimetry (DSC) were performed with a NETZSCH STA 409 PC/PG Luxx thermal analyzer. These measurements were carried out at an argon flow rate of $50\ ml \cdot min^{-1}$ and a heating rate of $5\ °C \cdot min^{-1}$. Morphology and solidity of the nanostructured copper particles on graphite were investigated by scanning electron microscopy (SEM) and energy dispersive X-ray spectroscopy (EDX) with a JEOL JSM-6700 F. An acceleration voltage of 2 kV was used for the SEM measurements and an acceleration voltage of 20 kV was used for the EDX measurements. Crystal structure investigations were carried out by powder X-ray diffraction (PXRD) using a STOE Stadi P PSD diffractometer utilizing Cu Kα radiation. The carbon content of the modified material was measured against the pristine material by a carbon analysis with an ELTRA CS-2000. These results were used to calculate the weight percentage of the copper particles on graphite.

4 Electrode preparation

Electrode tapes for battery cycling were prepared using a composition of 90 wt. % of synthetic graphite (either pristine or copper coated graphite), 5 wt. % of con-

ductive carbon black agent C-nergyTM Super C65 (TIMCAL) and 5 wt. % of sodium carboxymethylcellulose (Na-CMC) as binder (WALOCEL CRT 2000 PPA 12, Dow Wolff Cellulosics). Prior to the dispersion of the solid compounds, the binder polymer was dissolved in deionized water to obtain a 2.5 wt. % solution. The appropriate amount of Super C65 was added to the binder solution and the mixture was further equilibrated.

Electrode tapes for cyclic voltammetry were prepared using a composition of 95 wt. % of synthetic graphite (either pristine or copper coated graphite) and 5 wt. % of polyvinylidene fluoride (PVDF) as binder (TIMCAL). The binder was solvated in N-Methyl-2-pyrrolidone (NMP).

The pristine or modified graphite was added to the binder solution and dispersed using a T 25 ULTRA-TURRAX (1 h, 5000 rpm) to eliminate possible agglomerates and homogenize the paste. Afterwards, the electrode paste was cast on a high purity copper foil (Carl Schlenk) using the doctor-blade technique. The gap of the doctor blade was chosen to be 100 µm leading to an average mass loading of 3 $mg \cdot cm^{-2}$. The tapes were immediately transferred into an atmospheric oven and dried for 12 h at 80 °C. A further drying step was done in a BÜCHI oven under an oil-pump vacuum ($< 10^{-1}$ mbar) at 170 °C for 24 h. Thereafter, the tapes were stored in an argon filled glove box (UniLab, MBraun) with water and oxygen contents below 1 ppm.

5 Electrochemical measurements

The electrochemical investigations were carried out in Swagelok type T-cells with a three electrode setup. The measurements were performed in a half-cell setup using high purity metallic lithium foil (Chemetall) both as reference and counter electrodes. As separator a stack of polypropylene fleeces (Freudenberg FS2190) for the battery cycling and a glass fiber separator (MACHEREY-NAGEL MN QF-10) for cyclic voltammetry, drenched with 120 µL of electrolyte, were used. The electrolyte used in all investigations was a 3 : 7 wt. % mixture of ethylene carbonate (EC) : diethylene carbonate (DEC) with 1 M $LiPF_6$ as conductive salt. The water content of the electrolytic solution determined by Karl Fischer titration was less than 10 ppm. Charge/discharge cycling was carried out using a multichannel MACCOR 4300 battery test system. The cyclic voltammetry measurements were carried out using a multichannel Bio-Logic VMP3 potentiostat. In order to promote stable SEI formation, the charge and discharge steps in the first three cycles were performed using a constant current which corresponds to a 0.1 C charge/discharge rate (lower cut-off potential of 20 mV vs. Li/Li^+; upper

cut-off potential of 1500 mV vs. Li/Li^+). Afterwards, the charging (lithiation) was performed using first a galvanostatic step with a current corresponding to a 1 C charge/discharge rate down to a cut-off potential of 20 mV vs. Li/Li^+, followed by a 1 h potentiostatic step at this potential. Discharging (delithiation) was performed at a constant current corresponding to 1 C up to a cut-off potential of 1500 mV vs. Li/Li^+.

6 Results and discussion

Figure 2 shows the TG/DSC results of the pyrolysis of copper formate in the temperature range from 75 °C to 300 °C. The TG curve displays three small weight loss steps between 75 °C and 90 °C, which are related to the loss of crystallization water. The second major weight loss step with an exothermic DSC signal at 215 °C is caused by the decomposition of the copper formate to elemental copper and gaseous byproducts. Calculations predicted a mass loss of 41% for this step, the measured mass loss amounts to 40%. As these values are in good agreement and no further mass loss steps are observed, it can be assumed that no other solid products than copper are obtained. Additionally, TG/DSC measurements point out that a synthesis temperature of at least 240 °C is required.

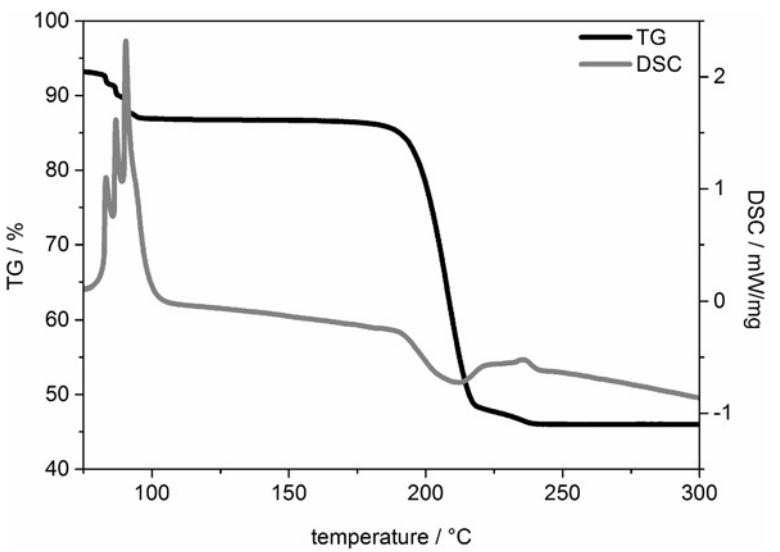

Figure 2: TG/DSC diagram of copper formate in a temperature range from 75 °C to 300 °C with a heating rate of $5\ °C \cdot min^{-1}$.

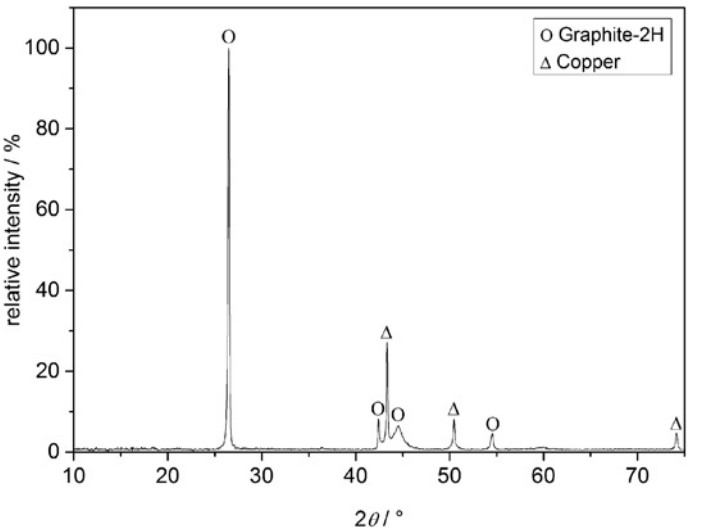

Figure 3: PXRD pattern of nanostructured copper particles on graphite.

PXRD was used to prove the identity of the synthesized nanostructured copper particles on graphite. The peaks at 2θ values of 26.4, 42.2, 44.4 and 54.5 degree refer to graphite while the peaks at 2θ values of 43.3, 50.4 and 74.1 degree belong to elemental copper and no further peaks are observed. Therefore, the PXRD pattern in Figure 3 demonstrates the phase purity of the copper particles within the detection limit of powder diffraction.

Figure 4 shows the SEM image of the pristine graphite. In the SEM image of the modified graphite in Figure 5a the copper particles appear as homogeneously distributed bright dots on the surface. The average diameter between 50 nm and 300 nm as well as the rosette crystal habit can be gathered from Figure 5b.

Figure 6 shows the locally resolved EDX spectrum for copper with its corresponding SEM image. It can be seen, that signals in the EDX correspond to the highlighted spots in the SEM image. Therefore, it can be assumed that the visible nanosized particles are copper depositions.

The expectation was to find an optimal weight percentage of copper that leads to an ideal electrochemical behavior. Cycling experiments with 2.7 wt. %, 4.5 wt. % and 7.5 wt. % of copper illustrate the limit range around this optimum. In the following section, data of electrochemical measurements of samples within this range is shown.

Important parameters to characterize the cycling behavior of electrodes are the Coulombic efficiency and the charge/discharge capacity [17]. Tables 1 and 2

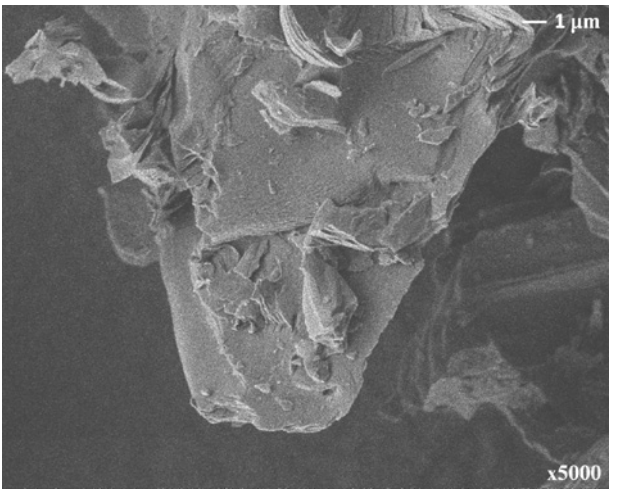

Figure 4: SEM image of pristine graphite at a magnification ratio of 5000.

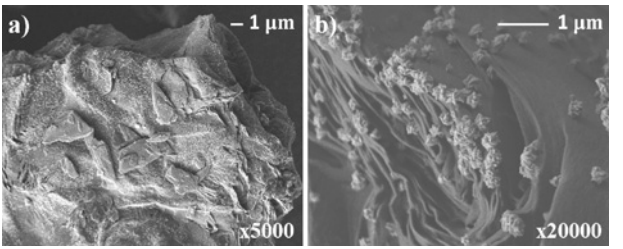

Figure 5: SEM image of a) nanostructured copper particles on graphite at a magnification ratio of 5000 and b) the rosette crystal habit at a magnification ratio of 20 000.

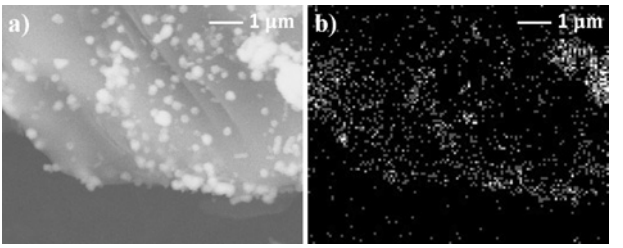

Figure 6: a) SEM image of nanostructured copper particles on graphite and b) locally resolved EDX measurement of copper.

display data for these characteristics obtained from representative cycles of charge/discharge measurements.

The Coulombic efficiency is slightly increased for the sample with 2.7 wt. % copper and slightly decreased for the other samples. The SEI formation takes place in the first few cycles. This causes an irreversible capacity loss and therefore a decreased Coulombic efficiency. It can be assumed from Table 1 that the SEI formation is increased for the samples with 4.5 wt. % and 7.5 wt. %. Thus, copper particles appear to support the SEI formation. As mentioned above, the SEI protects

Table 1: Coulombic efficiencies of representative charge/discharge cycles of pristine graphite and nanostructured copper particles on graphite with different weight percentages, obtained from constant current-constant voltage cycling data.

cycle	Coulombic efficiency / %			
	pristine graphite	2.7 wt. %	4.5 wt. %	7.5 wt. %
1st	82	85	79	79
2nd	97	98	95	97
3rd	98	99	98	98

Table 2: Specific discharge capacities of representative charge/discharge cycles of pristine graphite and nanostructured copper particles on graphite with different weight percentages, obtained from constant current-constant voltage cycling data.

cycle	discharge capacity / $mA \cdot h \cdot g^{-1}$			
	pristine graphite	2.7 wt. %	4.5 wt. %	7.5 wt. %
1st	226	311	312	282
100th	141	300	312	290
200th	93	287	311	272

the active material from cointercalation of solvated lithium ions. This leads to an increased cycle stability due to suppressed exfoliation. After 200 cycles the discharge capacity of the pristine graphite is strongly decreased to 93 $mA \cdot h \cdot g^{-1}$, whereas the discharge capacity of the copper coated graphite stays nearly constant, especially for the sample with 4.5 wt. % of copper (Table 2).

From Figure 7 and Table 2 it is obvious that the prepared composite materials show an increased discharge capacity compared to pristine graphite. Additionally to the enhanced SEI formation, it is possible that the copper particles improve the electronic conductivity in the sample, which facilitates the lithium ion transport at the interface. These could be some of the reasons for the increased capacity.

Considering these results, we found an optimal electrochemical performance for samples with copper contents between approximately 3 wt. % and 5 wt. %. Therefore, further investigations were carried out with samples within this range.

The total charge capacity can be separated into the charge capacity obtained in the constant current step and the charge capacity obtained in the constant voltage step. For the pristine graphite the main charge capacity is obtained in the constant voltage step, whereas the capacity from the constant current step is only about 50 $mA \cdot h \cdot g^{-1}$ (at the beginning of cycling) and is further decreasing upon cycling. For the prepared composite materials this effect dramatically changes as the main charge capacity of about 240 $mA \cdot h \cdot g^{-1}$ is obtained in the constant

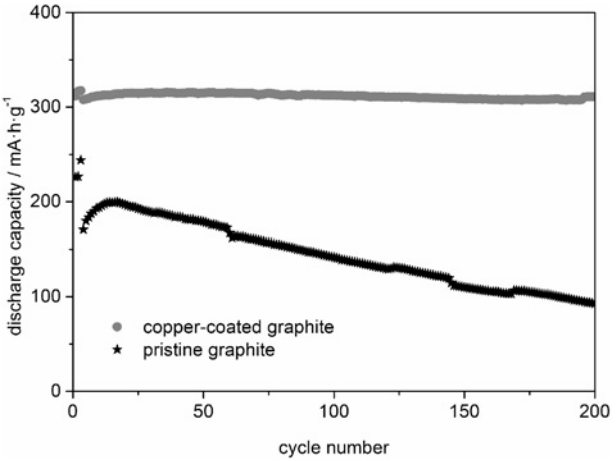

Figure 7: Constant current-constant voltage charge/discharge cycling curves of pristine graphite and a sample with nanostructured copper particles (4.5 wt. %) on graphite.

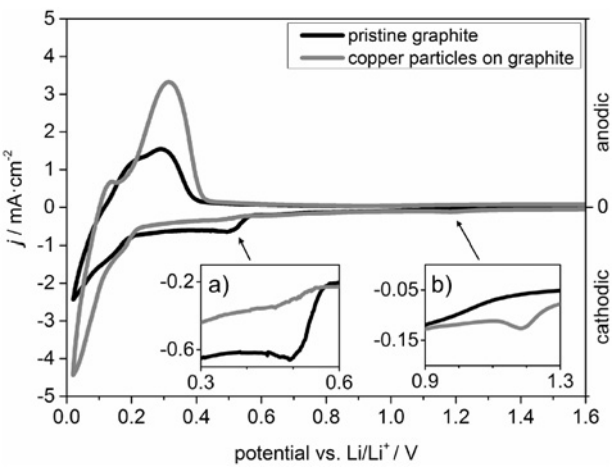

Figure 8: Cyclic voltammograms of pristine graphite and graphite with nanostructured copper particles (5.1 wt. %) on the surface in 1 M $LiPF_6$ EC/DEC 3 : 7 at a scan rate of 0.2 $mV \cdot s^{-1}$ between 0.02 V and 2.0 V. Comparison of the 1st cycles. The enlarged picture detail a) displays the cointercalation of solvated lithium ions and b) shows the SEI formation.

current step, whereas only a lower, but not negligible capacity increase of about 70 $mA \cdot h \cdot g^{-1}$ is gained by the constant voltage step.

Cyclic voltammetry is another method to characterize the electrochemical behavior of battery materials. Figure 8 presents the first cycles of the investigation of pristine graphite and of graphite with nanostructured copper particles on the surface via cyclic voltammetry. The pristine graphite shows one irreversible cathodic peak in the region between 0.3 V and 0.6 V and the anodic and cathodic

pair of peaks for the redox reaction of Li/Li^+ between 0.1 V and 0.3 V. The modified graphite shows a pair of peaks in a similar potential range. An additional weak peak appears at approximately 1.2 V.

Winter et al. reported that the cathodic peak between 0.3 V and 0.6 V corresponds to the cointercalation of solvated lithium ions [12]. This leads to a volume expansion of up to 200% compared to only 10% volume expansion for the intercalation of unsolvated lithium ions. Due to this, the material is exposed to mechanical stress which leads to exfoliation. As mentioned before, Guo et al. reported the suppression of solvated lithium ion cointercalation into graphite by copper coating [19]. The inset a) in Figure 8 shows the corresponding potential range of this reaction. As one can see, the corresponding cathodic current density of the modified graphite is clearly decreased compared to the pristine material. This implies a reduction of solvated lithium cointercalation. From the inset b) in Figure 8 it is observable that the cyclic voltammetry measurements show that there is an increased SEI formation during the first cycle which takes place in the potential range from 1.15 V to 1.25 V vs. Li/Li^+. These results indicate the enhancement of the SEI by copper coating and demonstrate its protective properties. They are in good agreement with the results of the charge/discharge cycling measurements.

7 Conclusions

By thermal decomposition of copper formate a homogeneous distribution of copper nanoparticles on graphite is obtained. In contradiction to other methods, all byproducts are gaseous and removed during the reaction. Therefore, it seems to be a good alternative to frequently used methods. The received modified material shows enhanced electrochemical properties both in charge/discharge cycling and cyclic voltammetry measurements. The main reason for the improvement seems to be an increased SEI formation which leads to a suppressed cointercalation of solvated lithium ions. In addition, the conductivity inside the electrode is improved, leading to a better charge transfer at the electrode surface. However, the mechanism for the formation of the SEI is still insufficiently understood and further investigations are necessary.

As mentioned before, graphite anodes show diverse advantages for the application in LIBs. Nevertheless, there are some problems which could be solved by metal coatings. The positive influence on the electrochemical properties of graphite might not be exclusive for copper coatings, it is also possible that other metal coatings show comparable improvements. Furthermore, studies on other metal coated electrode materials could be of broad interest.

Being simple and cost-efficient, the synthesis method presented here has the potential for industrial application. To transfer the method from laboratory scale to pilot-plant scale further investigations are clearly necessary.

Acknowledgement: The authors would like to thank the Ministry for Science and Culture of Lower Saxony (MWK) for financial support within the project Graduiertenkolleg Energiespeicher und Elektromobilität Niedersachsen (GEENI, ZN2783) and the Münster Electrochemical Energy Technology (MEET) for battery cycling. We gratefully acknowledge the supply of materials by SGL CARBON SE (Germany), TIMCAL Ltd. (Switzerland) and Chemetall GmbH (Germany). B. K. Licht and F. Homeyer contributed equally to this work.

References

1. M. Armand and J.-M. Tarascon, Nature **451** (2008) 652.
2. R. Marom, S. F. Amalraj, N. Leifer, D. Jacob, and D. Aurbach, J. Mater. Chem. **21** (2011) 9938.
3. B. Scrosati and J. Garche, J. Power Sources **195** (2010) 2419.
4. M. M. Thackery, C. Wolverton, and E. D. Isaacs, Energy Environ. Sci. **5** (2012) 7854.
5. M. Winter, J. O. Besenhard, M. E. Spahr, and P. Novák, Adv. Mater. **10** (1998) 725.
6. J. B. Goodenough and Y. Kim, Chem. Mater. **22** (2010) 587.
7. H. Wenzel, A. Haubrock, and H.-P. Beck, Z. Phys. Chem. **227** (2013) 57.
8. V. A. Sethuraman, L. J. Hardwick, V. Srinivasan, and R. Kostecki, J. Power Sources **195** (2010) 3655.
9. L. J. Hardwick, M. Marcinek, L. Beer, J. B. Kerr, and R. Kostecki, J. Electrochem. Soc. **155** (2008) A442.
10. P. Arora and R. E. White, J. Electrochem. Soc. **145** (1998) 3647.
11. J. Vetter, P. Novák, M. R. Wagner, C. Veit, K.-C. Möller, J. O. Besenhard, M. Winter, M. Wohlfahrt-Mehrens, C. Vogler, and A. Hammouche, J. Power Sources **147** (2005) 269.
12. M. Winter, P. Novák, and A. Monnier, J. Electrochem. Soc. **145** (1998) 428.
13. Ph. Bernardo, J. Dentzer, R. Gadiou, W. Märkle, D. Goers, P. Novák, M. E. Spahr, and C. Vix-Guterl, Carbon **49** (2011) 4867.
14. M. Winter, Z. Phys. Chem. **223** (2009) 1395.
15. Y. P. Wu, E. Rahm, and R. Holze, J. Power Sources **114** (2003) 228.
16. H. Huang, E. M. Kelder, and J. Schoonman, J. Power Sources **97/98** (2011) 114.
17. M. Inagaki, Carbon, **50** (2012) 3247.
18. H. Nozaki, K. Nagaoka, K. Hoshi, N. Ohta, and M. Inagaki, J. Power Sources **194** (2009) 486.
19. K. Guo, Q. Pan, L. Wang, and S. Fang, J. Appl. Electrochem. **32** (2002) 679.
20. W. Lu, V. S. Donepudi, J. Prakash, J. Liu, and K. Amine, Electrochim. Acta **47** (2002) 1601.
21. J. K. Lee, D. H. Ryu, J. B. Ju, Y. G. Shul, B. W. Cho, and D. Park, J. Power Sources **107** (2002) 90.

22. Y. Wu, C. Jiang, C. Wan, and E. Tsuchida, Electrochem. Commun. **2** (2000) 626.
23. S. Goriparti, E. Miele, F. De Angelis, E. Di Fabrizio, R. P. Zaccaria, and C. Capiglia, J. Power Sources **257** (2014) 421.
24. A. A. Vecher, S. V. Dalidovich, and E. A. Gusev, Thermochim. Acta **89** (1985) 383.
25. H. Wang, Y. Huang, Z. Tan, and X. Hu, Anal. Chim. Acta **526** (2004) 13.
26. R. G. Herman, K. Klier, G. W. Simmons, B. P. Finn, and J. B. Bulko, J. Catal. **56** (1979) 407.
27. H. Kobayashi, N. Takezawa, and C. Minochi, J. Catal. **69** (1981) 487.